

Surgical therapy of advanced ligature-induced peri-implantitis defects: cone-beam computed tomographic and histological analysis

Frank Schwarz, Narja Sahm, Ilja Mihatovic, Vladimir Golubovic and Jürgen Becker

Department of Oral Surgery, Heinrich Heine University, Düsseldorf, Germany

Schwarz F, Sahm N, Mihatovic I, Golubovic V, Becker J. Surgical therapy of advanced ligature-induced peri-implantitis defects: cone-beam computed tomographic and histologic analysis. *J Clin Periodontol* 2011; 38: 939–949. doi: 10.1111/j.1600-051X.2011.01739.x.

Abstract

Objectives: To evaluate radiological bone level (RBL) (i.e. cone-beam computed tomography) and histological bone levels (HBL) as well as re-osseointegration [bone-to-implant contact (BIC)] after surgical resective (i.e. implantoplasty) and/or regenerative therapy of advanced ligature-induced peri-implantitis in dogs.

Material and methods: At all defect sites ($n = 6$ dogs, $n = 48$ implants), the intrabony component was filled with a particulate bovine-derived natural bone mineral (NBM). The supracrestal component was treated by either the application of an equine bone block (EB) or implantoplasty.

In a split-mouth design, NBM and EB were soak-loaded with recombinant human bone morphogenetic protein (rhBMP)-2 or sterile saline. All sites were covered by a native collagen membrane and left to heal in a submerged position for 12 weeks.

Results: A premature wound exposure was observed at nine defect sites. Mean RBL and HBL values were lowest in the P+rhBMP-2 group, reaching statistical significance when compared with the EB group. Mean BIC values were comparable in all groups. Within-group comparisons commonly revealed a close correlation between RBL and HBL values.

Conclusions: It was concluded that (i) in all groups the investigations failed to predictably obtain complete defect resolution, (ii) the surgical procedure was associated with high exposure rates, and (iii) RBL was closely correlated with HBL.

Key words: bone graft; collagen membrane; implantoplasty; peri-implantitis; surgical regenerative therapy

Accepted for publication 2 May 2011

Conflict of interest and source of funding statement

The authors declare that they have no conflict of interests related to this study.

The study was funded by the Osteology Foundation, Lucerne, Switzerland, and the Camlog Foundation, Basel, Switzerland. The study materials and devices were kindly provided by Camlog Biotechnologies AG, Basel, Switzerland, Geistlich Biomaterials, Wolhusen, Switzerland, and Orangedental, Biberach, Germany.

In recent years, the treatment of infectious diseases affecting osseointegrated implants in function has become a demanding issue in implant dentistry. Peri-implant mucositis describes an inflammatory lesion that resides in the mucosa, while peri-implantitis also affects the supporting bone (Heitz-Mayfield 2008). It has been reported that peri-implantitis lesions in both dogs and humans most commonly featured a combined (79%) defect configuration

including a supracrestal as well as an intrabony aspect (Schwarz et al. 2007). When clinical signs suggest the presence of peri-implantitis, it is recommended to take a radiograph of the site to confirm the diagnosis (Lindhe & Meyle 2008). Even though intra-oral radiography (IR) and panoramic radiography are the most commonly used techniques, their diagnostic accuracy is limited to two planes, thus preventing the evaluation of crestal bone-level

changes at vestibular and oral aspects. In contrast, computed tomography (CT) and cone-beam computed tomography (CBCT) allow the evaluation of the implant supporting alveolar bone in several orthogonal planes. However, due to the higher radiation exposure of CT scans and the better imaging quality of CBCT scans around dental implants (Mengel et al. 2006), the use of the latter seems to be advantageous for the diagnosis of peri-implantitis defects. While IR has also been routinely used to evaluate bone-level changes after surgical therapy of peri-implantitis (Schwarz et al. 2006), CBCT has not been validated for this indication.

Some evidence suggests that mucositis lesions are reversible (Lang & Berglundh 2011, Salvi et al. 2011); however, non-surgical therapy of peri-implantitis was not found to be effective (Lindhe & Meyle 2008). In contrast, access flap surgery (AFS) was associated with a resolution of the inflammatory cell infiltrate, and in case of a submerged healing procedure, promotion of new bone fill and a certain re-establishment of new bone-to-implant contact (BIC). Basically, surgical therapy of peri-implantitis may be accomplished by using resective and/or regenerative approaches (Claffey et al. 2008, Schwarz et al. 2011). Several experimental and clinical studies assessed the effects of regenerative treatment procedures at intrabony defect components (Claffey et al. 2008, Renvert et al. 2009); however, a promising long-term stability (i.e. 4 years) has, so far, only been documented for a natural bone mineral (NBM) in combination with the principle of guided bone regeneration (Schwarz et al. 2009b). In contrast, there are only very few data available aimed at investigating potential treatment approaches for the supra-crestal component of peri-implantitis lesions. The treatment of these vertical bone defects with resective surgery and implantoplasty was evaluated in two publications (Romeo et al. 2005, 2007), indicating that this treatment approach led to clinical and radiological improvements over a period of 3 years. Up to now, there is only one experimental study available reporting on vertical bone regeneration in peri-implantitis defects after the implantation of recombinant human (rh) bone morphogenetic protein (BMP)-2 soaked on an absorbable collagen sponge in monkeys (Hanisch et al. 1997). It was

observed that rhBMP-2 promoted bone formation and re-osseointegration in comparison with the uncoated vehicle carrier (Hanisch et al. 1997). Recently, an equine-derived collagen containing cancellous bone block (EB) was introduced in order to provide an improved scaffold to support bone regeneration at advanced ridge defects (Fontana et al. 2008, Simion et al. 2009, Schwarz et al. 2010). A precursor of EB was characterized by less osteoconductive properties, but was proven to act as an alternative scaffold for the delivery of rhBMP-2 in various types of defect models (Jung et al. 2003, Schwarz et al. 2008). On the basis of these findings, the application of a soak-loaded EB might be a valuable alternative to an implantoplasty for the surgical regenerative therapy of advanced peri-implantitis defects. This issue, however, has not been addressed in previous studies.

Therefore, the aim of the present experimental study was to evaluate the impact of rhBMP-2 on the radiological (i.e. CBCT) and histological outcome of a combined surgical approach using NBM (i.e. intrabony component) either with EB or implantoplasty (i.e. supra-crestal component) for the treatment of ligature-induced peri-implantitis lesions in dogs.

Materials and Methods

Animals

A total of six beagle dogs, aged 14–16 months (mean weight 31.6 ± 2.9 kg), were included in the study. All animals exhibited a fully erupted permanent dentition. During the experiment, the dogs were fed once per day with soft-food diet and water *ad libitum*. Animal selection, management, and surgery protocol were approved by the Animal Care and Use Committee of the Heinrich Heine University and the local government. The experimental segment of the study started after an adaptation period of 4 weeks.

Study design

The study was performed in four phases.

In the first phase, the mandibular and maxillary 1st, 2nd, 3rd, 4th premolar as well as 1st and 2nd molar (P1–M2) were extracted. After a healing period of 10 weeks, titanium implants were bilaterally placed in the lower jaws ($n = 8$ per animal) and left to heal in a non-submerged position for 6 weeks. Subsequently, advanced peri-implantitis lesions were induced by ligature place-

ment in the lower jaws. All defects were treated with AFS, including granulation tissue removal and surface debridement/decontamination using plastic curets + cotton pellets soaked in sterile saline. After a meticulous assessment of the intrabony (i) and supra-crestal (s) defect components (Schwarz et al. 2007), the experimental sites were randomly and equally allocated in a split-mouth design to account for the influence of rhBMP-2 in the following groups: (1) particulate bovine-derived NBM (i)/EB (s), or (2) particulated NBM (i)/implantoplasty (s). Following grafting, a native collagen membrane (CM) was trimmed and adapted over each defect site. Accordingly, the following groups were tested on two implants of each animal ($n = 6$):

- NBM (i)/EB (s)+CM (two defects) (referred to as EB)
- NBM (i)/implantoplasty (s)+CM (two defects) (referred to as P)
- NBM+rhBMP-2 (i)/EB+rhBMP-2 (s)+CM (two defects) (referred to as EB+rhBMP-2)
- NBM+rhBMP-2 (i)/implantoplasty (s)+CM (two defects) (referred to as P+rhBMP-2)

The animals were euthanized after 12 weeks of submerged healing.

Configuration assessment of peri-implant bone defects

During AFS, the supraalveolar and intrabony components of the defects (Schwarz et al. 2007) were measured by one blinded and previously calibrated investigator (I. M.) using a periodontal probe (PCP 12, Hu-Friedy, Tuttingen, Germany) at four aspects (mesial, distal, vestibular, oral) (Fig. 1):

1. supra-crestal component (referred to as Class II) – of the defect, measured as maximum linear distance from the borderline between the implant shoulder (IS) and the alveolar bone crest, and
2. intrabony component of the defect (referred to as Class I), measured as the linear distance from the alveolar bone crest to the bottom of the defect.

Intra-operative assessment of the defect configuration revealed the following classes:

Class Ib (i.e. buccal dehiscence + semicircular bone resorption to the middle of the implant body)

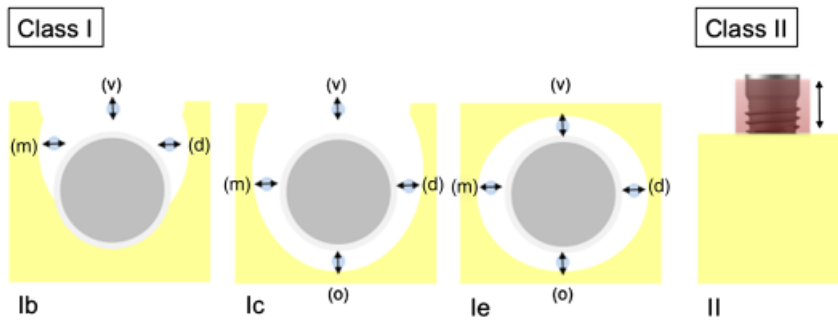


Fig. 1. Intra-operative assessment of the defect components. Class I: Intrabony component. Class Ib (i.e. buccal dehiscence+semicircular bone resorption to the middle of the implant body). Class Ic (i.e. buccal dehiscence+circular bone resorption under maintenance of the lingual compacta). Class Ie (i.e. circular bone resorption under maintenance of the buccal and oral compacta). Intrabony component (i) = blue circles; Circumferential (i.e. width) components (c) = arrows; m = mesial aspect; d = distal aspect; v = vestibular aspect; and o = oral aspect; Class II: Supracrestal component (s) = arrow. The red rectangle indicates the surface areas undergoing an implantoplasty.

Table 1. Distribution and baseline defect characteristics in mm (mean \pm SD)

Group	Class Ib	Class Ic	Class Ie	s(a) (mm)*	s(c) (mm)*	i (mm)*
EB	1	4	4	4.4 \pm 1.1	1.3 \pm 0.7	1.8 \pm 1.2
P	3	3	5	3.6 \pm 1.2	0.8 \pm 0.8	1.2 \pm 1.0
EB+rhBMP-2	2	3	4	3.5 \pm 1.4	1.4 \pm 0.9	2.1 \pm 1.6
P+rhBMP-2	3	3	4	3.4 \pm 1.5	1.4 \pm 0.9	1.9 \pm 1.4

*Comparisons between groups (unpaired *t*-test): NS.

s(a), supraalveolar component; s(c), circumferential component (i.e. width); i, intrabony component; EB, equine bone block; P, implantoplasty; rhBMP-2, recombinant human bone morphogenetic protein.

Class Ic (i.e. buccal dehiscence+circular bone resorption under maintenance of the lingual compacta), and Class Ie (i.e. circular bone resorption under maintenance of the buccal and oral compacta).

The baseline defect characteristics in different groups are presented in Table 1.

Surgical procedure

Before each surgical intervention, intramuscular sedation was accomplished with 0.17 mg/kg acepromazine (Vetranquil 1%, Ceva Tiergesundheits, Düsseldorf, Germany). Subsequently, anaesthesia was initiated using 21.5 mg/kg thiopental-sodium (Trapanal 2.5%, Altana GmbH, Konstanz, Germany). During all surgical procedures, inhalation anaesthesia was performed using oxygen, nitrous oxide, and isoflurane. To maintain hydration, all animals received a constant rate infusion of lactated Ringer's solution while anaesthetized. Intra-operative analgesia was performed by intravenous injection of 0.4 mg/kg piritramid (Dipidorol[®], Janssen-Cilag GmbH, Neuss, Germany) and 4.5 mg/kg carprofene (Rimadyl[®], Pfizer Pharma GmbH, Karlsruhe, Germany). For post-opera-

tive treatment, piritramid and carprofene were applied subcutaneously for 3 days in the same dose as described before.

Phase 1: tooth extraction

In the first surgery, P1–M2 were carefully removed bilaterally in the upper and lower jaws after reflection of mucoperiosteal flaps and tooth separation. After wound closure by means of mattress sutures, the sites were allowed to heal for 10 weeks. Prophylactic administration of clindamycine (11.0 mg/kg body weight, Cleorobe[®], Pharmacia Tiergesundheits, Erlangen, Germany) was performed intra-operatively and post-operatively for 10 days.

Phase 2: implant placement

In the second surgery, midcrestal incisions were made and mucoperiosteal flaps were reflected to expose the respective sites for implant insertion in the lower jaw. Surgical implant sites were prepared bilaterally, at a distance of 10 mm apart, using a low-trauma surgical technique under copious irrigation with sterile 0.9% physiological saline (Becker et al. 2007). Particular care was taken to preserve a residual

thickness of the alveolar bone crest of at least 2 mm at both buccal and lingual aspects of each implant site. All implants (\varnothing 3.8 mm, length: 11 mm, Camlog[®] Screw-Line Implant, Promote[®] plus, Camlog Biotechnologies AG, Basel, Switzerland) were inserted with good primary stability (i.e. lack of clinical mobility) in a way so that IS exceeded the buccal aspect of the alveolar crest for 0.4 mm (ID), as suggested in the surgical protocol of the manufacturer. Matching wide-body healing abutments (\varnothing 3.8 mm, height: 4.0 mm, Camlog) were connected (torque: 15 Ncm) immediately after implant placement in both groups. Following irrigation, mucoperiosteal flaps were repositioned with mattress sutures (Resorba[®], Nürnberg, Germany), and implants were left to heal in a non-submerged position. In order to prevent a trauma to the peri-implant mucosa, oral hygiene procedures were omitted during the initial healing period of 7 days. Thereafter, a plaque control programme including tooth and implant cleaning by the use of a toothbrush was initiated and performed twice per week without anaesthesia.

Phase 3: experimental peri-implantitis

After 6 weeks of healing, cotton ligatures (4–0) were placed in a submarginal position around each implant according to a method described previously (Lindhe et al. 1992) and the plaque control regimen was terminated. In brief, ligatures were forced into a position directly apical of the mucosal margin. Subsequently, a 'pocket' was created, which enabled the establishment of a submucosal microflora. The ligatures were exchanged once every 4 weeks and removed when approximately 60% of the initial bone support was lost on the basis of the evaluation of standardized radiographs (Schwarz et al. 2006). This active break down period of 4 months was followed by a progression period of 4 weeks and supported by a renewal of the plaque control regimen (i.e. teeth and abutments were cleaned with a toothbrush and dentifrice) (Lindhe et al. 1992).

Soak-loading of the vehicle carriers

The lyophilized differentiation factor rhBMP-2 (InductOs[®], Wyeth Pharma GmbH, Muenster, Germany) was dissolved in sterile water for injection

according to the instructions given by the manufacturer. For soak-loading of the particulated graft, 0.5 g NBM was moistened with 0.67 ml of a 0.77 mg/ml rhBMP-2 solution, while the control samples were moistened with 0.67 ml of sterile saline alone. Similarly, EB was soak-loaded with 2.3 ml of a 0.77 mg/ml rhBMP-2 solution (1.77 mg rhBMP-2 per block), while the control samples were moistened with 2.3 ml of sterile saline alone (Schwarz et al. 2008, 2009a). Soak-loaded and control NBM/EB were implanted after a rehydration time of 15 min, respectively.

Phase 4: treatment of peri-implantitis defects

Mucoperiosteal flaps were raised buccally and orally by means of intra-circumferential incisions under general anaesthesia. Subsequently, carbon curets (Institut Straumann AG, Basel, Switzerland) were used to completely remove all granulation tissue from the defect area as well as for a thorough debridement of the titanium implant surfaces. Afterwards, soaked cotton pellets were homogeneously adapted to all exposed implant surface areas and used under moderate pressure to remove all remaining non-mineralized deposits, which was followed by a thorough irrigation with sterile saline.

In respective groups, an implantoplasty was performed at supracrestally (i.e. Class II) exposed implant surfaces in a way as to completely planish the threatened areas and smoothen the structured implant surface using diamant burrs (ZR Diamonds, Gebr. Brasseler GmbH & Co. KG, Lemgo, Germany) and arkansas stones under copious irrigation with sterile saline. Particular care was taken to completely remove any metal deposits from the surrounding tissues. In all groups, NBM (BioOss[®] spongiosa granules, particle size 0.25–1 mm, Geistlich Biomaterials, Wolhusen, Switzerland) was applied in a way as to homogeneously fill the intrabony defect component. Each EB block (Geistlich prototype block, width: 10 mm, thickness: 5 mm, height: 10 mm, Geistlich Biomaterials) was size adapted to the respective sites. In particular, its height was adapted to the supraalveolar component, its width to the circumferential component of the defect, and its depth to the bucco-lingual extension of the alveolar ridge. A central core (\varnothing 3.8 mm) was prepared

using the respective conventional rotating pilot and twist drills in ascending order and securely supported a rotational stability after EB block application at each specific site (Fig. 2a–f). Following grafting, a bioresorbable type I/III CM of porcine origin (BioGide[®], Geistlich Biomaterials) was trimmed and adapted over each defect site so as to cover 2–3 mm of the surrounding alveolar bone and to ensure stability of the graft material. Neither sutures nor pins were used for membrane fixation or stabilization (Fig. 2g). Finally, the mucoperiosteal flaps were repositioned coronally and fixed with vertical or horizontal mattress sutures in a way to ensure a submerged healing procedure (Fig. 2h). All treatments were performed by the same experienced surgeon (F. S.). Prophylactic administration of clindamycine (11.0 mg/kg body weight, Cleorobe[®], Pharmacia Tiergesundheit) was performed intra-operatively and post-operatively for 10 days.

Retrieval of specimens

The animals were killed (overdose of 3% sodium pentobarbital) after a healing period of 12 weeks, and the oral tissues were fixed by perfusion with 10% buffered formalin administered through the carotid arteries. The jaws were dissected and blocks containing the experimental specimens were obtained. All specimens were fixed in 10% neutral-buffered formalin solution for 4–7 days.

CBCT

For radiological analysis, CBCT (Pax-Duo 3D, Orangedental, Biberach, Germany) was used. For radiological assessment, the jaws were positioned with the help of a plastic container in order to provide a platform for a reproducible positioning. The laser orientation beam was used to align the jaws accurately in a reproducible position. The exposure settings selected for CBCT were 90 kV, 3.1 mA with a voxel size of 0.2 × 0.2 mm, an acquisition time of 15 s, and a field of view of 12 cm × 8.5 cm. The three-dimensional reconstructions as well as the original two-dimensional projections were saved in a proprietary data format file on the Intel Xeon 2.4 GHz PC system (Intel, Santa Clara, CA, USA) with 3.23 GB RAM. The measurements were performed using the Ez3D2009 imaging

software version 1.2.1.0 (Vatech Co. Ltd., Seoul, Korea).

For each experimental site, one sagittal image was assessed by selecting the most central aspect of each implant on the axial view under standardized conditions. These conditions included computer hardware, which was technically approved for radiological observations, and working in a room equipped with window shades and dimmable light allowing a standardized low-light ambience illumination. The computer was a 2.4 GHz Intel Xenon PC system (Intel, Santa Clara, CA, USA) with 3.23 GB RAM. The data were presented on a monitor of 19" in diagonal and having a resolution of 1280 × 1024 pixels (HP Compaq LA 1951g, Hewlett-Packard, Böblingen, Germany).

The following landmarks were identified in the sagittal images of each site: IS, and the most coronal level of radiological bone in contact with the implant [i.e. radiological bone level (RBL)]. Linear measurements were made by drawing a vertical line, following the long axis of the implant, from IS to RBL at two aspects (i.e. vestibular, oral).

Histological preparation

The specimens were dehydrated using ascending grades of alcohol and xylene, infiltrated, and embedded in methylmethacrylate (Technovit 9100 NEU, Heraeus Kulzer, Wehrheim, Germany) for non-decalcified sectioning. During this procedure, any negative influence of polymerization heat was avoided due to a controlled polymerization in a cold atmosphere (−4°C). After 20 h, the specimens were completely polymerized. Each implant site was cut in the vestibulo-oral direction along with the long axis of the implant using a diamond band saw (Exakt[®], Apparatebau, Nordstedt, Germany). Serial sections were prepared from the central defect area, resulting in two to four sections of approximately 300 μm in thickness each (Donath 1985). Only implant sections showing an inner thread were chosen for the histological evaluation. Subsequently, all specimens were glued with acrylic cement (Technovit 7210 VLC, Heraeus Kulzer, Wehrheim, Germany) to silanized glass slides (Super Frost, Menzel GmbH, Braunschweig, Germany) and ground to a final thickness of approximately 40 μm. All sections were stained with toluidine blue to

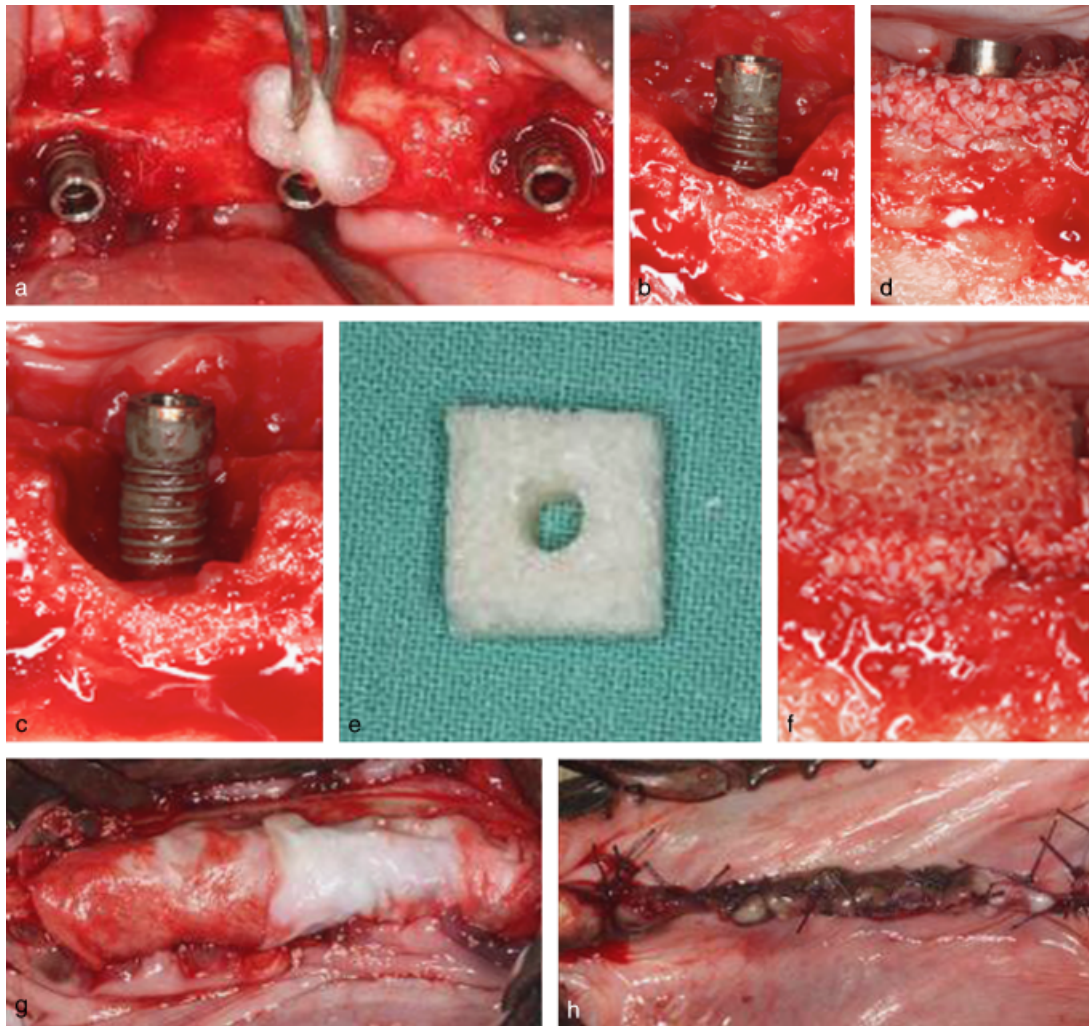


Fig. 2. Combination therapy at Class I and Class II defect components. (a) In all groups, granulation tissue removal and surface debridement were accomplished using carbon curets. For surface decontamination, CPS was homogeneously adapted to all exposed implant surface areas and used under moderate pressure to remove all remaining non-mineralized deposits, which was followed by a thorough irrigation with sterile saline. (b) Class Ie+II defect configuration. (c) Class Ic+II defect configuration. (d) NBM was applied in a way as to homogeneously fill the intrabony defect component. Implantoplasty was performed at supracrestally exposed implant surfaces in both P and P+rhBMP-2 groups. (e) EB was size-adapted and prepared by a central core (\varnothing 3.8 mm) using conventional rotating pilot and twist drills in ascending order consistent with the implant diameter. (f) EB was adapted with a rotational stability to the supraalveolar component in both EB and EB+rhBMP-2 groups. (g) CM was applied at each defect site as to cover 2–3 mm of the adjacent alveolar bone. (h) Experimental sites were left to heal in a submerged position for 12 weeks.

evaluate new bone formation. With this technique, old bone stains light blue, whereas newly formed bone stains dark blue because of its higher protein content (Schenk et al. 1984).

Histomorphometrical analysis

For image acquisition, a colour CCD camera (Color View III, Olympus, Hamburg, Germany) was mounted on a binocular light microscope (Olympus BX50, Olympus). Digital images (original magnification $\times 200$) were evaluated using a software program (Cell D[®], Soft Imaging System, Münster, Germany).

The following landmarks were identified in the stained sections at both vestibular and oral aspects: the IS, the bottom of the bone defect (BD), and the most coronal level of bone in contact with the implant surface [i.e. histological bone level (HBL)]. Linear measurements were made by drawing a vertical line, following the long axis of the implant, from IS to BD [i.e. defect length (DL)] and IS to HBL at two aspects (i.e. vestibular, oral). Percentage linear histological defect fill (PLHF) was calculated as $HBL/DL \times 100$. The amount of new BIC (i.e. the length proportion of the implant surface that was in direct contact with mineralized

tissue) was measured as a percentage of the distance from BD to IS, serving as 100% (Figs 4–5).

Intra-examiner reproducibility

Radiological and histological measurements were performed by one experienced investigator masked to the specific experimental conditions (N. S.). Before the start of the analyses, a calibration procedure was initiated for the investigator and revealed that repeated measurements of $n = 12$ different CBCT images and histological sections were similar at $>95\%$ level, respectively.

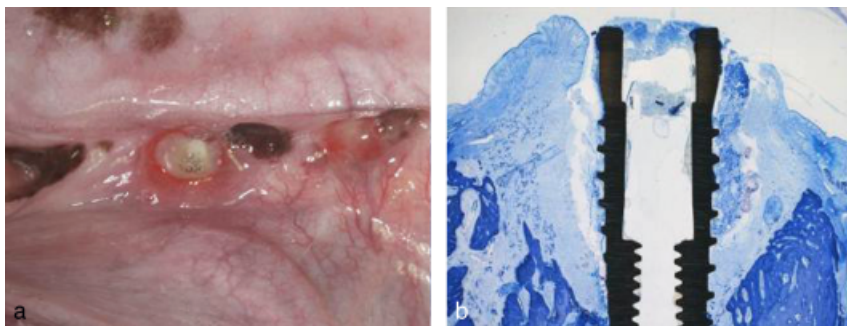


Fig. 3. Wound healing at 12 weeks. (a) A premature wound exposure was observed in three dogs, exhibiting a total of $n = 9$ experimental sites (for details, please refer to Table 3). (b) Histological analysis of exposed implant sites revealed a pronounced inflammatory cell infiltrate, which was associated with bone resorption extending to the apical region (P+rhBMP-2, corresponds to defect shown in Fig. 2b, original magnification $\times 25$).

Statistical analysis

The statistical analysis was performed using a commercially available software program (PASW Statistics 19.0, SPSS Inc., Chicago, IL, USA). Mean values and standard deviations among animals were calculated for each variable and group. The data rows were examined with the Kolmogorov–Smirnow test for normal distribution. For the comparisons between groups at 12 weeks, the unpaired *t*-test was used. The α -error was set at 0.05. The paired *t*-test was used for comparisons within groups (i.e. radiological versus histological data). The α -error was set at 0.05.

Results

Clinical healing

No complications such as allergic reactions, swellings, abscesses, or infections were observed throughout the whole study period. A premature exposure of the wound area was observed in three dogs, exhibiting a total of $n = 9$ experimental sites [EB: three sites; P: one site; EB+rhBMP-2: three sites; P+rhBMP-2: two sites (Fig. 3a)]. The radiological and histological analysis of these sites revealed a pronounced peri-implant bone resorption, extending to the apical region of respective implants (Fig. 3b).

Semi-quantitative CBCT and histological analysis

Histological observation of all groups investigated revealed different patterns of a bony filling of the secluded wound area confined by CM. While these changes were mainly related to the intrabony aspect at P and P+rhBMP-2-treated sites, both EB and EB+rhBMP-

2 groups also exhibited varying amounts of bone formation at the supracrestal defect component. The maturity of the woven bone was identifiable by the development of primary osteons and appeared to be comparable in both augmented and pristine areas. Basically, all CBCT images were characterized by minor beam-hardening artefacts, resulting in an imprecise depiction of either the bone implant interface or the borderline between intrabony and supracrestal defect components in the EB and EB+rhBMP-2 groups. However, the image quality of the crestal bone level was generally considered as good in the sagittal images of each site. Double contours were generally not observed (Figs 4 and 5).

In particular, EB and EB+rhBMP-2 groups were commonly characterized by a pronounced degradation of EB specimens, which revealed an interconnective, lacuna-like macroporous trabecular structure. In the EB group, residues of the scaffold were predominantly invaded by a vascularized fibrous connective tissue and frequently separated from the adjacent alveolar bone (Fig. 4a). A deposition of parallel-fibered woven bone in close contact to EB and subsequently the adjacent titanium implant surfaces were only observed occasionally and appeared to be limited to the basal compartment of the supracrestal defect component (Fig. 4a and c). At both intrabony and supracrestal defect components, bone formation and graft integration (i.e. EB and NBM) mainly originated from open marrow spaces of the adjacent alveolar bone (Fig. 4d).

The amount and extent of bone ingrowth and BIC consistently appeared to be higher in all EB+rhBMP-2 speci-

mens. However, only one out of the evaluated specimens revealed an almost complete osseous organization of the former defect area (Fig. 4e and f).

At P and P+rhBMP-2-treated sites, a dispersion of NBM particles was a frequent finding in most of the specimens evaluated (Fig. 5a). However, in contrast to the P group, a dispersion of NBM particles was occasionally associated with a vertical bone formation at P+rhBMP-2-treated sites (Fig. 5c and d). In both groups, the intrabony defect component was characterized by varying amounts of bone deposition in close contact to residual NBM particles and subsequently the adjacent titanium implant surfaces (Fig. 5a–d).

Implantoplasty was commonly associated with a slight to moderate deposition of titanium particles in the adjacent subepithelial connective tissue. These areas were demarcated by a localized mixed chronic inflammatory cell infiltrate mainly containing lymphocytes and plasma cells. In general, the inflammatory cell infiltrate seemed to be encapsulated by deposition of irregular bundles of fibrous connective tissue showing increased proliferation of vascular structures (Fig. 5e and f). In the entire FOV, CBCT analysis failed to reveal any identifiable dispersion of titanium particles derived from either P or P+rhBMP-2 groups.

Quantitative CBCT and histological analysis

The mean values of DL, RBL, HBL, PLHF, and BIC in different groups are presented in Table 2. After 12 weeks of healing, all groups revealed comparable mean DL values. Even though these values tended to be highest in the EB, and lowest in the P groups, these differences did not reach statistical significance ($p > 0.05$; unpaired *t*-test, respectively).

Lowest RBL and HBL values were observed in the P+rhBMP-2 group. This was followed by both EB+rhBMP-2 and P groups, showing comparable but lower RBL and HBL values when compared with EB-treated sites. Statistical analysis revealed a significant difference in mean HBL values between EB and P+rhBMP-2 groups ($p < 0.05$; unpaired *t*-test) (Table 2). Both P+rhBMP-2 and EB+rhBMP-2-treated sites tended to reveal higher mean PLHF and BIC values when compared with EB and P groups. However, a

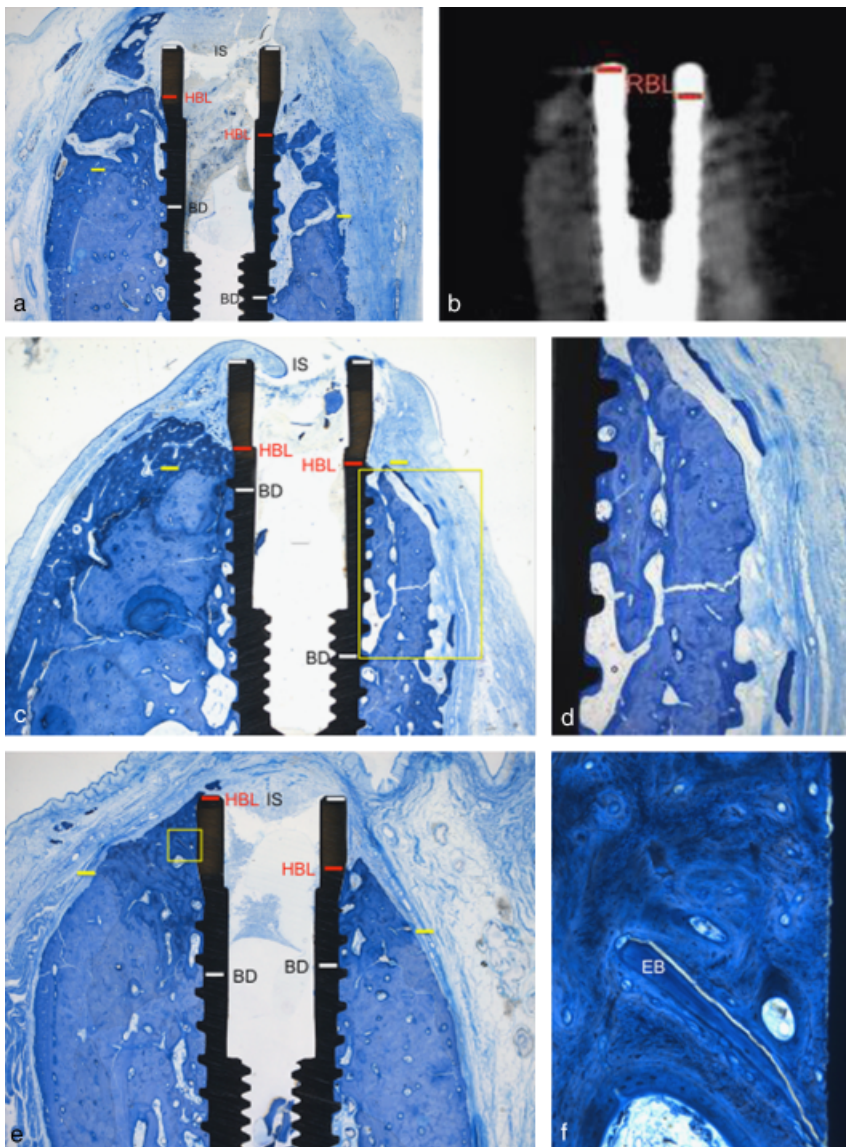


Fig. 4. CBCT digital images and histological views (vestibular aspects: right/oral aspects: left) of EB and EB+rhBMP-2 groups at 12 weeks. (a) EB blocks commonly revealed a pronounced degradation, and were also associated with a vertical bone formation (EB, corresponds to defect shown in Fig. 2c, original magnification $\times 25$). (b) Corresponding CBCT scan indicating an overestimation of RBL (red lines) in relation to HBL at both vestibular (right) and oral (left) aspects. Beam-hardening artefacts were minimal. (c) Bone formation at both suprabony and intrabony aspects originated from the adjacent alveolar bone. The perforation of the supporting mucosa was caused during histological processing (EB, original magnification $\times 25$). (d) Higher magnification view of the yellow box area shown in (c) indicating the establishment of new BIC (EB, original magnification $\times 100$). (e) Bone formation and BIC commonly appeared to be higher in the EB+rhBMP-2 group. An almost complete osseous organization of the former wound area was only observed in this specimen (EB+rhBMP-2, original magnification $\times 25$). (f) Higher magnification view of the yellow box area shown in (e) pointing to a deposition of new bone to residues of EB (EB+rhBMP-2, original magnification $\times 400$). Red line: histological (HBL)/radiological (RBL) bone level. Yellow line: borderline between intrabony and supracrestal defect components. IS, implant shoulder; BD, bottom of the defect; EB, equine-derived bone block.

statistically significant difference was only observed in mean PLHF values between EB and P+rhBMP-2 groups ($p < 0.05$; unpaired *t*-test) (Table 2). The mean values of DL, RBL, HBL,

PLHF, and BIC at either exposed or non-exposed sites in different groups are presented in Tables 3 and 4. In particular, at exposed sites, mean RBL values ranged from 7.0 ± 1.5 mm in the

P+rhBMP-2 group to 8.7 ± 2.5 mm in the EB+rhBMP-2 group, corresponding to mean HBL values of 6.6 ± 1.0 mm and 8.1 ± 1.6 mm, respectively (Table 3). At non-exposed sites, mean RBL values ranged from 1.5 ± 1.0 mm in the EB+rhBMP-2 group to 3.1 ± 0.8 mm in the EB group, corresponding to mean HBL values of 2.9 ± 0.8 mm and 4.0 ± 1.0 mm, respectively (Table 4).

Correlation between CBCT and histological analysis

Within-group correlations between RBL and HBL values at either vestibular sites or oral sites are presented in Table 5. Basically, CBCT analysis most frequently resulted in an overestimation of HBL at the vestibular aspects, while an underestimation was commonly observed at the corresponding oral aspects.

A close correlation between RBL and HBL values was commonly observed in EB, P, and P+rhBMP-2 groups at both vestibular and oral aspects ($p > 0.05$; paired *t*-test, respectively). In contrast, EB+rhBMP-2 (vestibular aspect)-treated sites were associated with a significant difference between RBL and HBL values ($p < 0.05$; paired *t*-test) (Figs 4a and b, 5a and b, Table 5).

Discussion

The present experimental study was designed to evaluate the impact of rhBMP-2 on the radiological and histological outcome of a surgical regenerative/resective approach combining particulated NBM either with EB or implantoplasty for the treatment of both intrabony and supracrestal components of ligatur-induced peri-implantitis defects in dogs.

Basically, quantitative analysis at 12 weeks has indicated that EB+rhBMP-2 and P+rhBMP-2 groups tended to be associated with higher PLHF and BIC values when compared with the EB and P groups. Even though between-group comparisons merely revealed a significant difference in mean HBL and PLHF values between EB and P+rhBMP-2 groups, the influence of rhBMP-2 on bone regeneration was distinctively observed in all specimens evaluated. The biological activity of rhBMP-2 soak-loaded NBM (1 mg rhBMP-2/g) has been proven in vitro as well as in experimental animal studies (Schwarz et al. 2008, 2009a). In contrast,

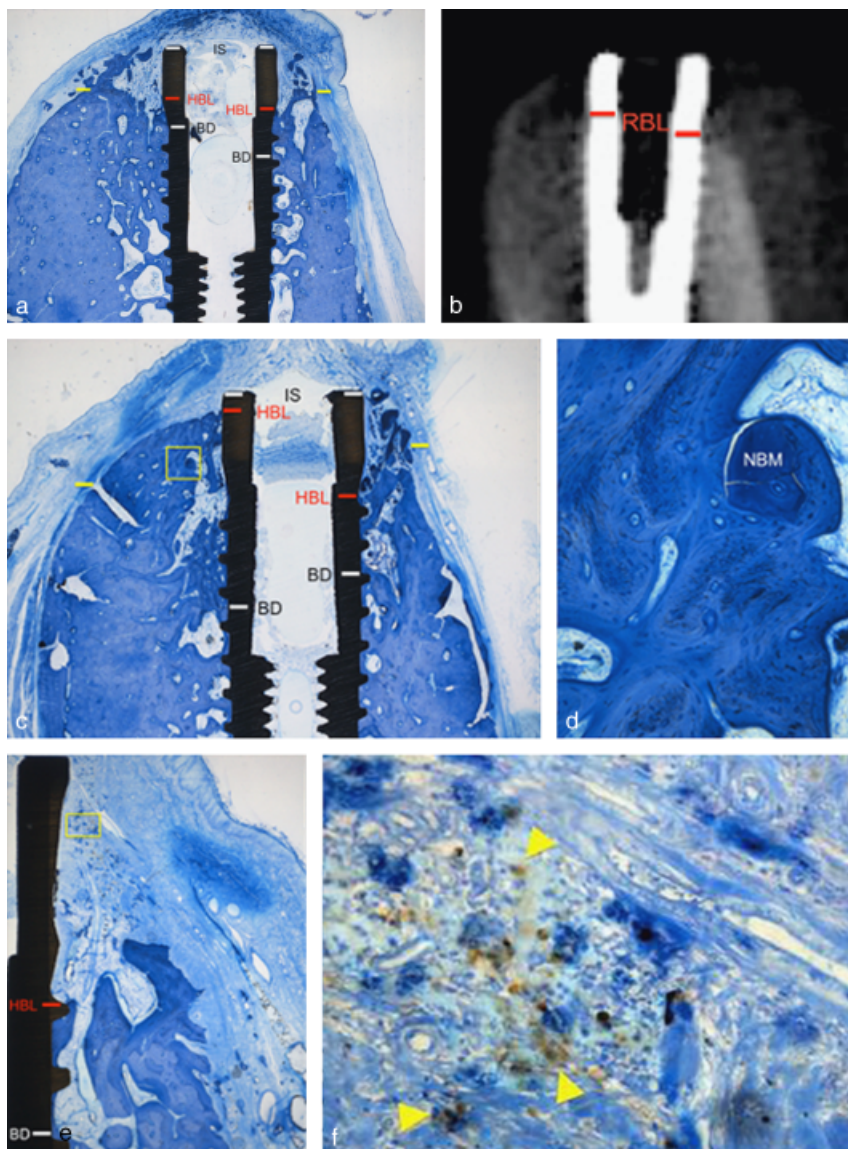


Fig. 5. CBCT digital images and histological views (vestibular aspects: right/oral aspects: left) of P and P+rhBMP-2 groups at 12 weeks. (a) A dispersion of NBM particles was a common finding in both groups (P, original magnification $\times 25$). (b) Corresponding CBCT scan indicating a correlation between RBL (red lines) and HBL (a) at both vestibular (right) and oral (left) aspects. (c) A vertical bone formation was also observed at P+rhBMP-2-treated sites (original magnification $\times 25$). (d) Higher magnification view of the yellow box area shown in (c) indicating osseous integration of dispersed NBM within the supracrestal defect component (P+rhBMP-2, original magnification $\times 100$). (e) The apical extension of the implantoplasty coincided with the crestal bone level. New bone formation and BIC were limited to the intrabony defect component (P+rhBMP-2, original magnification $\times 40$). (f) Higher magnification view of the yellow box area shown in Fig. 5e, pointing to a moderate deposition of titanium particles (arrowheads) in the subepithelial connective tissue. These areas were highly vascularized and demarcated by a mixed chronic inflammatory cell infiltrate (P+rhBMP-2, original magnification $\times 400$). Red line: histological (HBL)/radiological (RBL) bone level. Yellow line: borderline between intrabony and supracrestal defect components. IS, implant shoulder; BD, bottom of the defect; EB, equine-derived bone block.

soak-loading of EB was performed according to a procedure recently established for a precursor NBM block (Schwarz et al. 2008). However, both types of xenogenic blocks basically

reveal potential differences in their physicochemical properties, which in turn might also have an influence on the release kinetics of rhBMP-2. Even though the biologic activity of the

rhBMP-2 soak-loaded NBM block has also been proven in one experimental animal study, it is impossible to estimate to what extent these data can be transferred to EB (Schwarz et al. 2008, 2009a). Basically, when interpreting the present results, one must realize that these are the first experimental data reporting on CBCT and histological analysis of surgical regenerative and/or resective therapy of ligature-induced peri-implantitis defects. In this context, it must be emphasized that a close correlation between RBL and HBL values was commonly observed in EB, P, and P+rhBMP-2 groups. In contrast, EB+rhBMP-2 groups were associated with a significant underestimation of RBL in relation to HBL, which appeared to be more pronounced at the vestibular aspects. The differences noted between these groups may primarily be related to the radiopaque properties of EB. In addition, the inhomogeneous osseous organization as well as pronounced degradation noted for EB on the histological level may also have contributed to the imprecise correlation between RBL and HBL values in the EB+rhBMP-2 group. Basically, the results of a previous study performed on native pig mandibles confirmed that CBCT scans displayed only a slight deviation in the extent of standardized peri-implant defects (i.e. mean deviation of 0.17 ± 0.11 mm) in comparison with direct measurements (Mengel et al. 2006). However, the occurrence of scattered radiation and beam-hardening artefacts has been reported to be a main limitation of CBCT, thus precluding an assessment of BIC unless there is an obvious peri-implant bone loss (Farman & Scarfe 2008). Basically, these findings were not supported by the radiological data noted at least in the EB, P, and P+rhBMP-2 groups, as minor beam-hardening artefacts as well as the presence of dispersed radiopaque NBM particles at the bone crest were still associated with a high precision of CBCT scans. In this context, it must also be noted that the resolution associated with the current voxel size of 0.2 mm may be appropriate for an accurate assessment of a cortical bone thickness between 0.3 and 3.7 mm (Razavi et al. 2010).

The results of a previous experimental animal study also provide some evidence that the adjunctive use of NBM+CM may result in varying amounts of bone fill and re-osseointegration at ligature-induced peri-implantitis defects (Nociti et al.

Table 2. Radiological and histomorphometrical parameters (mean \pm SD) in different groups at 12 weeks: exposed and non-exposed sites ($n = 6$ animals)

Group	DL (mm)	RBL (mm)	HBL (mm)	PLHF (%)	BIC (%)
EB	5.8 \pm 1.6	4.7 \pm 2.5	5.1 \pm 1.8*	13.4 \pm 11.9*	13.1 \pm 12.3
P	4.6 \pm 1.4	3.4 \pm 1.8	3.9 \pm 1.7	17.4 \pm 15.8	13.7 \pm 11.4
EB+rhBMP-2	5.5 \pm 1.9	3.3 \pm 3.5	4.2 \pm 2.5	25.8 \pm 21.2	21.1 \pm 20.0
P+rhBMP-2	4.6 \pm 1.9	2.9 \pm 3.2	3.2 \pm 2.3	31.8 \pm 28.1	26.8 \pm 28.1

*Comparisons between groups (unpaired *t*-test): EB versus P+rhBMP-2 ($p < 0.05$).

DL, defect length; RBL, radiological bone level; HBL, histological bone level; PLHF, percentage linear histologic defect fill; BIC, bone-to-implant contact; EB, equine bone block; rhBMP-2, recombinant human bone morphogenetic protein.

Table 3. Radiological and histomorphometrical parameters (mean \pm SD) in different groups at 12 weeks: exposed sites ($n = 9$)

Group	DL (mm)	RBL (mm)	HBL (mm)	PLHF (%)	BIC (%)
EB ($n = 3$)	7.2 \pm 0.7	7.9 \pm 0.9	7.2 \pm 0.7	0	0
P ($n = 1$)	6.3	7.1	6.3	0	0
EB+rhBMP-2 ($n = 3$)	8.1 \pm 1.6	8.7 \pm 2.5	8.1 \pm 1.6	0	0
P+rhBMP-2 ($n = 2$)	6.6 \pm 1.0	7.0 \pm 1.5	6.6 \pm 1.0	0	0

DL, defect length; RBL, radiological bone level; HBL, histological bone level; PLHF, percentage linear histologic defect fill; BIC, bone-to-implant contact; EB, equine bone block; rhBMP-2, recombinant human bone morphogenetic protein.

Table 4. Radiological and histomorphometrical parameters (mean \pm SD) in different groups at 12 weeks: non-exposed Sites ($n = 39$)

Group	DL (mm)	RBL (mm)	HBL (mm)	PLHF (%)	BIC (%)
EB ($n = 9$)	5.1 \pm 1.4	3.1 \pm 0.8	4.0 \pm 1.0	20.1 \pm 8.4	19.7 \pm 9.4
P ($n = 11$)	4.5 \pm 1.4	3.1 \pm 1.4	3.7 \pm 1.6	19.0 \pm 15.5	15.0 \pm 11.0
EB+rhBMP-2 ($n = 9$)	4.6 \pm 1.1	1.5 \pm 1.0	2.9 \pm 0.8	34.4 \pm 16.7	28.1 \pm 18.1
P+rhBMP-2 ($n = 10$)	4.2 \pm 1.8	2.1 \pm 2.9	2.5 \pm 1.8	38.1 \pm 26.3	32.1 \pm 27.8

DL, defect length; RBL, radiological bone level; HBL, histological bone level; PLHF, percentage linear histological defect fill; BIC, bone-to-implant contact; EB, equine bone block; rhBMP-2, recombinant human bone morphogenetic protein.

Table 5. Within group correlations between radiological and histological bone levels (mean \pm SD in mm) at 12 weeks: exposed and non-exposed sites ($n = 6$ animals)

Group	RBL-v	HBL-v	Δ	RBL-o	HBL-o	Δ
EB	5.4 \pm 1.9	5.2 \pm 1.6	0.2 \pm 0.8	4.7 \pm 2.5	4.9 \pm 2.0	-0.2 \pm 0.7
P	4.4 \pm 1.4	4.0 \pm 1.7	0.4 \pm 1.0	3.4 \pm 1.8	3.7 \pm 1.8	-0.3 \pm 0.6
EB+rhBMP-2	3.7 \pm 3.1	4.6 \pm 2.1	-0.8 \pm 1.2*	3.3 \pm 3.5	3.8 \pm 2.9	-0.5 \pm 0.9
P+rhBMP-2	3.8 \pm 2.9	3.4 \pm 2.1	0.3 \pm 1.4	2.9 \pm 3.2	2.9 \pm 2.8	-0.1 \pm 1.0

*Comparisons between groups (paired *t*-test): $p < 0.05$.

Δ : RBL - HBL (positive/negative values represent an overestimation/underestimation of RBL in relation to HBL, respectively).

DL, defect length; RBL, radiological bone level; HBL, histological bone level; v, vestibular aspect; o, oral aspect; EB, equine bone block; rhBMP-2, recombinant human bone morphogenetic protein.

2000). In particular, an air powder flow was used for the decontamination of acid-etched titanium implants, which were subsequent to the application of NBM+CM, left to heal in a submerged position for 5 months. The histomorphometric evaluation revealed no significant differences with respect to bone formation and BIC at sites receiving either surface

debridement alone (49.5%/26.8%), CM alone (51%/26.6%), NBM alone (55.7%/28%), or a combination of NBM+CM (48%/25.6%) (Nociti et al. 2000). A radiographic evaluation of these findings was only performed in one publication (Schou et al. 2003). In particular, Schou et al. (2003) used standardized IR for quantitative digital subtraction radiography at 6

months after NBM application (surface decontamination: gauze soaked alternately in 0.1% aqueous chlorhexidine and saline) with or without an expanded polytetrafluorethylene (ePTFE) membrane in cynomolgus monkeys. The mean radiographic bone level gain at both mesial and distal aspects in the NBM group with and without ePTFE membrane varied between 5.0 and 4.6 mm, respectively (initial bone loss of 4.5–5 mm). This was associated with BIC values ranging from 36% (with ePTFE) to 14% (without ePTFE; value was estimated from data provided in the publication). Histologically, NBM particles were in general highly integrated within the regenerated bone, but the particles in the occlusal part of the defects were entirely surrounded by connective tissue irrespective of membrane coverage (Schou et al. 2003). Basically, mean BIC values as reported by Nociti et al. (2000) and Schou et al. (2003) appeared to be higher than the values noted in the present study. In this context, it must be emphasized that both publications did not report on the baseline defect characteristics. However, the intra-operative views provided in one original paper (Schou et al. 2003) seem to indicate that at least NBM+ePTFE was used for an augmentation of both intrabony and supracrestal defect components. The latter was intentionally approached by an implantoplasty in both P and P+rhBMP-2 groups of the present study, thus resulting in a decreased implant surface area where a new BIC may be accomplished (Albouy et al. 2011). In this context, it is also important to emphasize that histological analysis commonly revealed a slight to moderate deposition of titanium particles in the adjacent tissue to defects treated with P and P+rhBMP-2, which was associated with a localized chronic inflammatory cell infiltrate. However, previous clinical studies have shown that these depositions may not be associated with any adverse events (Romeo et al. 2007, Schwarz et al. 2011), indicating the safety and efficacy of an implantoplasty to serve as an alternative approach for the treatment of supracrestal defect components.

The observation that rhBMP-2 has the potential to promote bone formation and re-osseointegration in advanced peri-implantitis defects is also in agreement with the results of a previous experimental study performed in monkeys (Hanisch et al. 1997). At 4 months of submerged healing, rhBMP-2 soaked on an absorbable sponge carrier

(1.5 mg/ml; 0.1 mg/defect) resulted in a significantly higher vertical bone gain (2.6 ± 1.2 versus 0.8 ± 0.8 mm) and reosseointegration ($40.0 \pm 11.0\%$ versus $8.9 \pm 7.8\%$) than the application of the carrier alone (Hanisch et al. 1997). Even though the fast resorbability of a collagen sponge may be advantageous to support bone formation in conjunction with rhBMP-2, its poor mechanical properties can compromise the outcome of healing at the supracrestal defect component. However, the present data have also pointed to a pronounced degradation of EB, which is in agreement with histological findings following lateral ridge augmentation in dogs. In particular, it was reported that EB specimens were characterized by a significantly increased cell- (i.e. osteoclasts and multinucleated giant cells) mediated degradation of the graft material at 12 weeks (Schwarz et al. 2010). Taking into account the residual defect areas and high exposure rates as noted in all groups investigated, one must consider that rough implant surfaces (i.e. EB and EB+rhBMP-2 groups) may be more susceptible to disease progression than smoothed surfaces (i.e. P and P+rhBMP-2). Accordingly, from a clinical point of view, P and P+rhBMP-2 may offer a better ratio of defect resolution to potential susceptibility towards re-infection of exposed surface areas than EB or EB+rhBMP-2. Even though P has recently been shown to be associated with clinical and radiological improvements at advanced peri-implantitis defects over a period of 6 months, the long-term stability of this approach still needs to be addressed (Schwarz et al. 2011).

Within the limitations of the present study, it was concluded that (i) in all groups investigations failed to predictably obtain complete defect resolution, (ii) the surgical procedure was associated with high exposure rates, and (iii) that RBL was closely correlated with HBL.

References

Albouy, J. P., Abrahamsson, I., Persson, L. G. & Berglundh, T. (2011) Implant surface characteristics influence the outcome of treatment of peri-implantitis: an experimental study in dogs. *Journal of Clinical Periodontology* **38**, 58–64.

Becker, J., Ferrari, D., Herten, M., Kirsch, A., Schaefer, A. & Schwarz, F. (2007) Influence of platform switching on crestal bone changes at non-submerged titanium implants: a histomorphometrical

study in dogs. *Journal of Clinical Periodontology* **34**, 1089–1096.

Claffey, N., Clarke, E., Polyzois, I. & Renvert, S. (2008) Surgical treatment of peri-implantitis. *Journal of Clinical Periodontology* **35**, 316–332.

Donath, K. (1985) The diagnostic value of the new method for the study of undecalcified bones and teeth with attached soft tissue (Säge-Schliff (sawing and grinding) technique). *Pathology Research and Practice* **179**, 631–633.

Farman, A. G. & Scarfe, W. C. (2008) What is cone-beam CT and how does it work? *Dental Clinics of North America* **52**, 707–730.

Fontana, F., Rocchietta, I., Dellavia, C., Nevins, M. & Simion, M. (2008) Biocompatibility and manageability of a new fixable bone graft for the treatment of localized bone defects: preliminary study in a dog model. *International Journal of Periodontics and Restorative Dentistry* **28**, 601–607.

Hanisch, O., Tatakis, D. N., Boskovic, M. M., Rohrer, M. D. & Wikesjö, U. M. (1997) Bone formation and reosseointegration in peri-implantitis defects following surgical implantation of rhBMP-2. *International Journal of Oral and Maxillofacial Implants* **12**, 604–610.

Heitz-Mayfield, L. J. (2008) Peri-implant diseases: diagnosis and risk indicators. *Journal of Clinical Periodontology* **35**, 292–304.

Jung, R. E., Glauser, R., Scharer, P., Hammerle, C. H., Sailer, H. F. & Weber, F. E. (2003) Effect of rhBMP-2 on guided bone regeneration in humans. *Clinical Oral Implants Research* **14**, 556–568.

Lang, N. P. & Berglundh, T. (2011) Peri-implant diseases - Consensus report of the 7th European Workshop on Periodontology. *Journal of Clinical Periodontology* **38** (Suppl. 11), 178–181.

Lindhe, J., Berglundh, T., Ericsson, I., Liljenberg, B. & Marinello, C. (1992) Experimental breakdown of peri-implant and periodontal tissues. A study in the beagle dog. *Clinical Oral Implants Research* **3**, 9–16.

Lindhe, J. & Meyle, J. (2008) Peri-implant diseases: Consensus Report of the Sixth European Workshop on Periodontology. *Journal of Clinical Periodontology* **35**, 282–285.

Mengel, R., Kruse, B. & Flores-de-Jacoby, L. (2006) Digital volume tomography in the diagnosis of peri-implant defects: an in vitro study on native pig mandibles. *Journal of Periodontology* **77**, 1234–1241.

Nociti, F. H. Jr., Caffesse, R. G., Sallum, E. A., Machado, M. A., Stefani, C. M. & Sallum, A. W. (2000) Evaluation of guided bone regeneration and/or bone grafts in the treatment of ligature-induced peri-implantitis defects: a morphometric study in dogs. *Journal of Oral Implantology* **26**, 244–249.

Razavi, T., Palmer, R. M., Davies, J., Wilson, R. & Palmer, P. J. (2010) Accuracy of measuring the cortical bone thickness adjacent to dental implants using cone beam computed tomography. *Clinical Oral Implants Research* **21**, 718–725.

Renvert, S., Polyzois, I. & Maguire, R. (2009) Reosseointegration on previously contaminated surfaces: a systematic review. *Clinical Oral Implants Research* **20** (Suppl. 4), 216–227.

Romeo, E., Ghisolfi, M., Murgolo, N., Chiapasco, M., Lops, D. & Vogel, G. (2005) Therapy of peri-implantitis with resective surgery. A 3-year clinical trial on rough screw-shaped oral implants. Part I: clinical outcome. *Clinical Oral Implants Research* **16**, 9–18.

Romeo, E., Lops, D., Chiapasco, M., Ghisolfi, M. & Vogel, G. (2007) Therapy of peri-implantitis with resective surgery. A 3-year clinical trial on rough screw-shaped oral implants. Part II: radiographic

outcome. *Clinical Oral Implants Research* **18**, 179–187.

Salvi, G. E., Aglietta, M., Eick, S., Sculean, A., Lang, N. P. & Ramseier, C. A. (2011) Reversibility of experimental peri-implant mucositis compared to experimental gingivitis in man. *Clinical Oral Implants Research* doi: 10.1111/j.1600-0501.2011.02220.x.

Schenk, R. K., Olah, A. J. & Herrmann, W. (1984) Preparation of calcified tissues for light microscopy. In: Dickson, G. R. (ed). *Methods of Calcified Tissue Preparation*, pp. 1–56. Amsterdam: Elsevier.

Schou, S., Holmstrup, P., Jorgensen, T., Skovgaard, L. T., Stoltze, K., Hjorting-Hansen, E. & Wenzel, A. (2003) Anorganic porous bovine-derived bone mineral (Bio-Oss) and ePTFE membrane in the treatment of peri-implantitis in cynomolgus monkeys. *Clinical Oral Implants Research* **14**, 535–547.

Schwarz, F., Ferrari, D., Balic, E., Buser, D., Becker, J. & Sager, M. (2010) Lateral ridge augmentation using equine- and bovine-derived cancellous bone blocks: a feasibility study in dogs. *Clinical Oral Implants Research* **21**, 904–912.

Schwarz, F., Ferrari, D., Sager, M., Herten, M., Hartig, B. & Becker, J. (2009a) Guided bone regeneration using rhGDF-5- and rhBMP-2-coated natural bone mineral in rat calvarial defects. *Clinical Oral Implants Research* **20**, 1219–1230.

Schwarz, F., Herten, M., Sager, M., Bieling, K., Sculean, A. & Becker, J. (2007) Comparison of naturally occurring and ligature-induced peri-implantitis bone defects in humans and dogs. *Clinical Oral Implants Research* **18**, 161–170.

Schwarz, F., Jepsen, S., Herten, M., Sager, M., Rothamel, D. & Becker, J. (2006) Influence of different treatment approaches on non-submerged and submerged healing of ligature induced peri-implantitis lesions: an experimental study in dogs. *Journal of Clinical Periodontology* **33**, 584–595.

Schwarz, F., Rothamel, D., Herten, M., Ferrari, D., Sager, M. & Becker, J. (2008) Lateral ridge augmentation using particulated or block bone substitutes bio-coated with rhGDF-5 and rhBMP-2: an immunohistochemical study in dogs. *Clinical Oral Implants Research* **19**, 642–652.

Schwarz, F., Sahn, N., Bieling, K. & Becker, J. (2009b) Surgical regenerative treatment of peri-implantitis lesions using a nanocrystalline hydroxyapatite or a natural bone mineral in combination with a collagen membrane: a four-year clinical follow-up report. *Journal of Clinical Periodontology* **36**, 807–814.

Schwarz, F., Sahn, N., Iglhaut, G. & Becker, J. (2011) Impact of the method of surface debridement and decontamination on the clinical outcome following combined surgical therapy of peri-implantitis: a randomized controlled clinical study. *Journal of Clinical Periodontology* **38**, 276–284.

Simion, M., Nevins, M., Rocchietta, I., Fontana, F., Maschera, E., Schupbach, P. & Kim, D. M. (2009) Vertical ridge augmentation using an equine block infused with recombinant human platelet-derived growth factor-BB: a histologic study in a canine model. *International Journal of Periodontics and Restorative Dentistry* **29**, 245–255.

Address:

Frank Schwarz
Department of Oral Surgery
Westdeutsche Kieferklinik
Heinrich-Heine-University
D-40225 Düsseldorf, Germany
E-mail: Frank.Schwarz@med.uni-duesseldorf.de

Clinical Relevance

Scientific rationale for the study: The impact of rhBMP-2 on the RBL and HBL after a combined surgical regenerative and resective therapy (i.e. particulate bovine-derived NBM at the intrabony component combined either with an equine bone block (EB) or implantoplasty (P) at the supracrestal component) of advanced ligature-induced peri-implantitis is unknown.

Principal findings: At 12 weeks after therapy, CBCT and histological analysis closely revealed that all groups investigated had a limited effect on mean RBL and HBL values and reosseointegration. Statistically significant higher HBL reductions were noted in the P+rhBMP-2 group when compared with EB-treated sites. The surgical procedure was associated with high exposure rates, as observed at nine defect sites.

Practical implications: P and P+rhBMP-2 may offer a better ratio of defect resolution to potential susceptibility towards re-infection of exposed surface areas than EB or EB+rhBMP-2. CBCT may represent an accurate diagnostic tool for the radiological assessment of HBL in peri-implantitis defects.

This document is a scanned copy of a printed document. No warranty is given about the accuracy of the copy. Users should refer to the original published version of the material.